



## Spatio-temporal patterns of stratification on the Northwest Atlantic shelf



Yun Li <sup>a,b,\*</sup>, Paula S. Fratantoni <sup>c</sup>, Changsheng Chen <sup>d</sup>, Jonathan A. Hare <sup>c</sup>, Yunfang Sun <sup>d</sup>, Robert C. Beardsley <sup>e</sup>, Rubao Ji <sup>b</sup>

<sup>a</sup> Integrated Statistics under Contract with NOAA NMFS, Northeast Fisheries Science Center, Woods Hole, MA 02543, USA

<sup>b</sup> Biology Department, Woods Hole Oceanographic Institution, Woods Hole, MA 02543, USA

<sup>c</sup> NOAA/NMFS, Northeast Fisheries Science Center, Woods Hole, MA 02543, USA

<sup>d</sup> School for Marine Science and Technology, University of Massachusetts–Dartmouth, New Bedford, MA 02744, USA

<sup>e</sup> Physical Oceanography Department, Woods Hole Oceanographic Institution, Woods Hole, MA 02543, USA

### ARTICLE INFO

#### Article history:

Received 18 June 2014

Received in revised form 9 January 2015

Accepted 10 January 2015

Available online 2 February 2015

### ABSTRACT

A spatially explicit stratification climatology is constructed for the Northwest Atlantic continental shelf using daily averaged hydrographic fields from a 33-year high-resolution, data-assimilated reanalysis dataset. The high-resolution climatology reveals considerable spatio-temporal heterogeneity in seasonal variability with strong interplay between thermal and haline processes. Regional differences in the magnitude and phasing of the seasonal cycle feature earlier development/breakdown in the Middle Atlantic Bight (MAB) and larger peaks on the shelf than in the Gulf of Maine (GoM). The relative contribution of the thermal and haline components to the overall stratification is quantified using a novel diagram composed of two key ratios. The first relates the vertical temperature gradient to the vertical salinity gradient, and the second relates the thermal expansion coefficient to the haline contraction coefficient. Two distinct regimes are identified: the MAB region is thermally-dominated through a larger portion of the year, whereas the Nova Scotian Shelf and the eastern GoM have a tendency towards haline control during the year. The timing of peak stratification and the beginning/end of thermally-positive and thermally-dominant states are examined. Their spatial distributions indicate a prominent latitudinal shift and regional-ity, having implications for the seasonal cycle of ecosystem dynamics and its interannual variability.

© 2015 Elsevier Ltd. All rights reserved.

### Introduction

In temperate coastal and shelf seas, density stratification exhibits a pronounced seasonal cycle, primarily associated with the seasonal variability in water temperature (Mayer et al., 1979; Beardsley et al., 1985; Linder and Gawarkiewicz, 1998). A traditionally accepted picture is that, a strong thermocline dominates the upper water column in spring and summer, predominantly forced by atmospheric heating at the surface. In fall and winter, stratification weakens as atmospheric heating decreases and surface wind stress strengthens, driving energetic vertical mixing and overturning. The tendency has been to view these governing processes in a one-dimensional (vertical) frame, where atmospheric heating/cooling and wind mixing dominate over other drivers in controlling the timing and magnitude of stratification. However, in a highly advective system such as the Northwest Atlantic continental shelf, horizontal heat and freshwater transport

also play a significant role in determining the magnitude, timing and distribution of stratification.

As atmospheric warming increases and freshwater export from the Arctic Ocean becomes more variable (e.g., Belkin et al., 1998), it is also likely that stratification in the Northwest Atlantic shelf region will be affected by the changing climate. It has been suggested that variations in the timing and magnitude of stratification may be responsible for driving changes in the seasonal cycles of nutrients, plankton, and higher-trophic-level consumers (MERCINA Working Group, 2012). Since seasonal changes lead the total variation to first order, a clearer understanding of the seasonal cycle of stratification and its predominant drivers can provide a mechanistic foundation for distinguishing geographic divisions and identifying distinct regimes in local variability. A more comprehensive understanding of seasonal stratification has emerged over the past three decades (e.g., Smith, 1989; Mountain and Manning, 1994; Lentz et al., 2003; Deese-Riordan, 2009; Castelao et al., 2010), leading to recognition of its complexity in general. In particular, seasonal changes on the shelf are dominated by two processes: riverine/oceanic sources (e.g., freshwater outflow, subpolar/subtropical oceanic sources, ice melt, etc.) regulate stratification through the advection of water with different

\* Corresponding author at: Biology Department, Woods Hole Oceanographic Institution, Woods Hole, MA 02543, USA.

E-mail address: [yli@whoi.edu](mailto:yli@whoi.edu) (Y. Li).

temperature and/or salinity characteristics, while atmospheric forcing (e.g., heating/cooling, precipitation/evaporation, wind-induced mixing) directly alters the density in the upper water column and ultimately contributes to stratification. These studies move away from the one-dimensional view of stratification, demonstrating that the effects of thermal and haline processes must be considered jointly in order to diagnose the regional heterogeneity of stratification magnitude and timing. For instance, [Mountain and Manning \(1994\)](#) noted that the seasonal timing of freshwater input to the GoM, coupled with the annual cycle in seasonal heating over the region, leads to asymmetries between the western and eastern GoM, with the western region (WGoM) being more strongly stratified in the summer and more vertically uniform in the winter than the eastern region (EGoM). [Castelao et al. \(2010\)](#) demonstrated that variations in near-surface salinity play a larger role in driving seasonal hydrographic variability in the central Middle Atlantic Bight (MAB) than in the northern MAB, and most of the variance is due to pulses in river discharge and the movement of the shelfbreak front.

Stratification is fundamental to a wide range of ecological processes, because it controls the availability of nutrients and light to surface primary producers (e.g., [Townsend, 1998](#)) and biological productivity. The spring phytoplankton bloom usually occurs as light availability increases, when the stratification-reduced mixed layer depth is shallower than the critical depth and nutrient concentrations are elevated throughout the water column following strong winter mixing ([Sverdrup, 1953](#)). Although this canonical view has been challenged recently as the dilution of grazers is considered (e.g., [Behrenfeld, 2010](#); [Boss and Behrenfeld, 2010](#)), stratification is still regarded as the key controlling process. The fall bloom, on the other hand, occurs when seasonally enhanced vertical mixing (convective cooling and winds) renews the nutrient supply in the euphotic zone before light availability becomes fully limiting ([Findlay et al., 2006](#); [Hu et al., 2011](#)).

An understanding of local stratification variability is an essential mechanistic foundation for assessing the marine ecosystem response to environmental variability. For example, the recruitment success of fish populations in the Gulf of Maine (GoM) might be related to salinity-induced changes in stratification, influencing phytoplankton production and zooplankton community structure (e.g., [Durbin et al., 2003](#); [Ji et al., 2007, 2008](#); [Kane, 2007](#); [Mountain and Kane, 2010](#)). A strong decadal-scale shift in copepod community structure was observed in the 1990s ([Pershing et al., 2005](#); [Kane, 2007](#)), when the ratio of small- to large-sized copepod species increased compared with the 1980s and 2000s. These changes in zooplankton community structure were linked to decreasing salinity and increasing stratification ([Kane, 2005](#)). In addition, the phytoplankton color index (PCI) and the diatom/dinoflagellate data from Continuous Plankton Recorder (CPR) measurements also showed decadal changes that are coincident with the changes in the zooplankton community ([Kane, 2011](#)). These changes in hydrography and plankton are associated with changes in the relative recruitment rate of cod and haddock in the fishery ecosystem of the Northwest Atlantic shelf ([Link et al., 2002](#); [Pershing et al., 2005](#); [Friedland et al., 2008](#); [Mountain and Kane, 2010](#)).

Most of our current knowledge on the magnitude and timing of seasonal stratification has been gained without fully addressing its spatio-temporal variability. This is a gross simplification for regions dominated by advective processes, having large gradients in hydrography (e.g., [Mountain, 2003](#)), and significant regional variability in the proximity of fresh water sources and upwelling/downwelling zones (e.g., [Castelao et al., 2008](#)). To date, our understanding of the spatio-temporal heterogeneity of seasonal stratification has been lacking due to the resolution of existing observations. Studies based on moored observations are well suited to addressing the temporal evolution but are limited spatially

(e.g. [Beardsley et al., 1985](#); [Lentz et al., 2003](#)), while hydrographic surveys resolve the spatial structure without adequately resolving the temporal transitions ([Linder and Gawarkiewicz, 1998](#); [Castelao et al., 2008](#)). Hydrographic measurements made by the National Oceanic and Atmospheric Administration, National Marine Fisheries Service represent the most comprehensive ongoing, shelf-wide record of hydrographic measurements on the Northeast U.S. continental shelf. However, shifts in sampling protocols, changes in instrument technology, and biases in sampling coverage/intervals inevitably complicate efforts to provide a spatially explicit map of stratification. Statistical estimates based on coherence scales of shelf-wide surveys are not constrained by dynamics and still only provide coarse regional estimates of stratification magnitude and timing (e.g., [Mountain et al., 2004](#); [Fratantoni et al., 2013](#)). While numerical ocean models have certainly contributed to our understanding of hydrographic variability in this region, observations are still needed to reduce the uncertainty in these models (e.g., [Han and Loder, 2003](#)).

While the interdisciplinary research community has a growing interest in the development of local stratification indices, one possible solution to fill the gap in our knowledge is to utilize a dynamic ocean model to constrain the interpolation of observational data and obtain a so-called “reanalysis” product. Reanalysis combines observations with a numerical model to produce four-dimensional fields that have high spatio-temporal resolution, which are physically consistent among different variables, and are constrained by the dynamical laws that govern the relationships between these variables. This approach allows all observations to be concentrated in a unified framework for easy quality control and assessment. In the atmospheric research field, reanalysis (e.g., National Centers for Environmental Prediction and the National Center for Atmospheric Research (NCEP/NCAR) Reanalysis) has been viewed revolutionary in providing uniformly mapped fields (without spatial or temporal gaps) of both observed and derived variables ([Carton and Giese, 2008](#)). Significant progress has also been made in global and quasi-global scale ocean climate reanalysis (see a list of available products at [http://iccd.zmaw.de/easy\\_init\\_ocean.html?&L=1](http://iccd.zmaw.de/easy_init_ocean.html?&L=1)).

To our knowledge, this study provides the first systematic examination of seasonal stratification in the Northwest Atlantic shelf region, where spatial and temporal scales are both simultaneously highly resolved. In order to characterize the magnitude and timing of stratification for the Northwest Atlantic shelf region, we take advantage of an FVCOM-based (Finite Volume Coastal Ocean Model; [Chen et al., 2003](#)) data-assimilative high-resolution product recently developed based on the Northeast Coastal Ocean Forecast System (NECOFS) ([http://fvcom.smast.umassd.edu/research\\_projects/NECOFS/index.html](http://fvcom.smast.umassd.edu/research_projects/NECOFS/index.html)). The remainder of the paper is organized as follows. Section ‘Study area’ provides a description of the study area. Section ‘Data and methodology’ describes the observations and reanalysis product used, gives three criteria to measure density stratification, and introduces a new regime diagram that can be used to gauge the relative importance of thermal and haline controls on stratification. Section ‘Results’ presents the spatio-temporal patterns of the overall stratification and its thermal and haline components, with focus on the magnitude and timing. Section ‘Discussion’ discusses the regimes distinguishing each region, examines possible drivers, and speculates on the implications for ecosystem dynamics. Finally, a summary is provided in Section ‘Summary’.

## Study area

The study area encompasses the shelf region between 38 and 45.5°N in the Northwest Atlantic ocean (referred as the Northwest

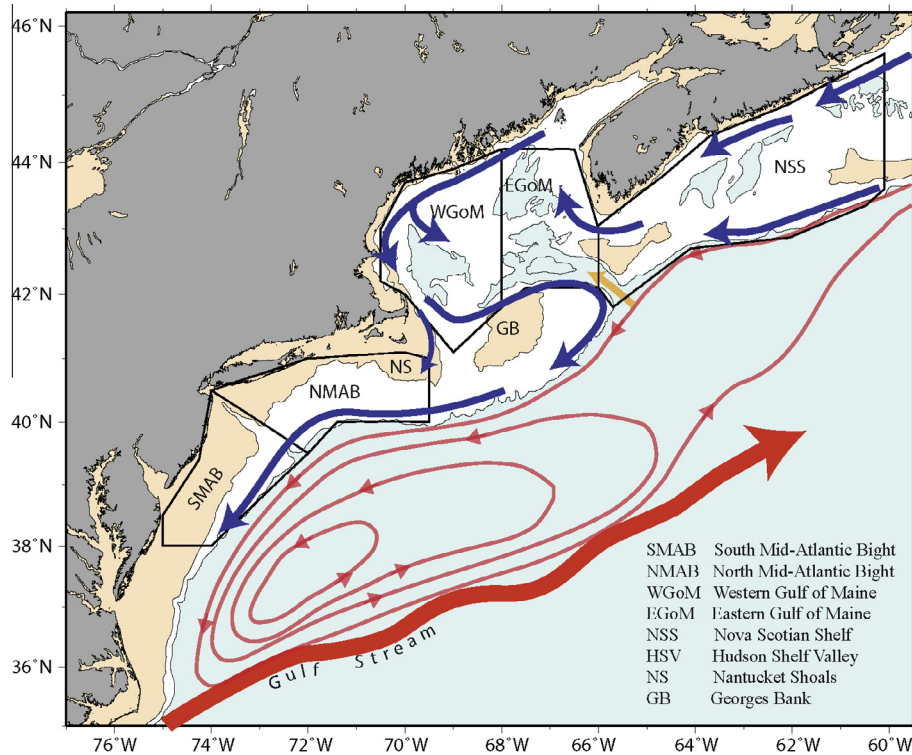


**Fig. 1.** Map of the Northwest Atlantic shelf region, showing major currents, with the colder, fresher shelf water in blue, and the warmer, saltier warm slope-sea water in red. Water depths <50 m are shaded light orange and >200 m are shaded light blue. The orange arrow delineates the deep Slope Water entering the Gulf of Maine (GoM) through the Northeast Channel. The boundaries of five subregions used in the analysis are also shown. The schematic circulation is based on numerous observations across this region (e.g., the slope water circulation follows the schematic representation by Csanady and Hamilton (1988), and the shelf circulation follows Butman and Beardsley (1992)). (For interpretation of the references to color in this figure legend, the reader is referred to the web version of this article.)

Atlantic Shelf hereafter), including the Nova Scotian Shelf (NSS), GoM, Georges Bank (GB) and MAB regions (see Fig. 1 for locations). Five subregions are defined based on oceanographic characteristics in order to examine some features on regional scales (cf., Mountain et al., 2004; Fratantoni et al., 2013). However, because GB is strongly mixed and weakly stratified throughout the year (see details in Fig. 4a–d), it is not considered in this study. In all five regions, the hydrographic properties exhibit pronounced season variations and are influenced by a variety of sources. This part of the continental shelf features an equatorward buoyancy-driven coastal current transporting cold, low-salinity water from higher latitudes. These waters, derived from remote sources (e.g., Belkin et al., 1998; Smith et al., 2001), traverse the NSS, circulating counter-clockwise around the GoM and clockwise around GB, before continuing southwestward through the MAB (e.g., Smith, 1983; Beardsley et al., 1985; Loder et al., 1998; Houghton and Fairbanks, 2001; Lentz, 2008). Warmer, saltier water resides immediately off-shelf in the adjoining slope-sea, bounding the colder, fresher shelf water and establishing a persistent thermohaline front at the shelf break along the length of the domain (Fratantoni and Pickart, 2003). This warmer, saltier oceanic water is a dominant source of deep water to the GoM, entering through the Northeast Channel and progressively flooding the deep basins therein (Ramp et al., 1985). Elsewhere, cross-shelf exchange periodically introduces this slope water into the shelf region along the frontal boundary (Linder and Gawarkiewicz, 1998; Lozier and Gawarkiewicz, 2001; Lentz, 2003). In addition, seasonal heating and cooling (e.g., Lentz et al., 2003; Castelao et al., 2008), wind-induced mixing and up- and downwelling (e.g., Petrie et al., 1987; Lentz et al., 2003; Deese-Riordan, 2009), river runoff from the coasts (referred to as local freshwater sources) (e.g., Lentz et al., 2003; Deese-Riordan, 2009; Taylor and Mountain, 2009;

Castelao et al., 2010) are all important. Those forcing mechanisms induce notable but different annual cycles in temperature and salinity within the upper water column, with their joint effects leading to the spatio-temporal heterogeneity of density stratification that has not been fully explored in previous studies (e.g., Lentz et al., 2003; Loder et al., 2003; Drinkwater and Gilbert, 2004; Deese-Riordan, 2009).

## Data and methodology

### Data

The data-assimilative high-resolution reanalysis database was created through hindcast NECOFS experiments (<http://porpoise1.smast.umassd.edu:8080/fvcomwms/>). The reanalysis database differs from mere observations, as it produces estimates of continuous data fields using a model with ocean dynamics to constrain the interpolation. The hydrodynamic model in NECOFS is the third generation of GoM-FVCOM with a computational domain encompassing the shelf region between 35 and 46°N in the Northwest Atlantic ocean (see Appendix for details). Assimilation was conducted regionally using optimal interpolation based on spatio-temporal scales determined from covariance analysis. The assimilated observation dataset consisted primarily of satellite-derived SST, temperature and salinity profile data whose distribution was concentrated along shipping routes and historically occupied stations. Stratification is one of the physical properties that is probably the most difficult to simulate, yet has important impact on biological processes. Prior to proceeding with the broader analysis, an assessment of the reanalysis product is conducted. It shows high correlation ( $r = 0.71$ – $0.95$ ) and small

errors ( $RMSD < 0.71$ ), except for moderate underestimation of the observed variability ( $NSTD < 1$ ) in five subregions. It is expected that the underestimation results from either the model vertical resolution, which is lower than the observations, or the embedded scheme, which tends to smooth the model density profiles. Overall, the model shows similar skill in capturing the stratification regardless of three different criteria (described later in Section ‘Stratification criteria’) used for the skill assessment (see Appendix for details).

### Stratification criteria

Stratification is defined by vertical density differences that are a consequence of vertical variations in temperature and salinity, and can be quantified using a number of criteria (Fig. 2). The buoyancy frequency or Brunt–Väisälä frequency  $N$  ( $s^{-1}$ ) is among the most commonly used indicators of stratification in oceanography, and is defined as (Gill, 1982),

$$N^2 = -\frac{g}{\rho} \frac{d\rho}{dz} \quad (1)$$

where  $g$  is the gravitational acceleration ( $m\ s^{-2}$ ),  $\rho$  is the density of sea water ( $kg\ m^{-3}$ ), and  $z$  is the vertical depth coordinate (meters). Positive (negative) values of  $N^2$  correspond to stable (unstable) stratified conditions. Stratification may also be defined based on the potential energy anomaly  $\phi$  ( $J\ m^{-3}$ ), so-called Simpson Energy, which represents the work required to break down vertical density differences and bring about complete mixing (Simpson et al., 1990). Despite the fact that stratification is influenced by three-dimensional processes, most of the seasonal stratification variability in this region is concentrated in the upper 50 m (see the Appendix for details), a feature that allows us to focus on the upper 50 m of the water column, assuming that the surface layer stratification will

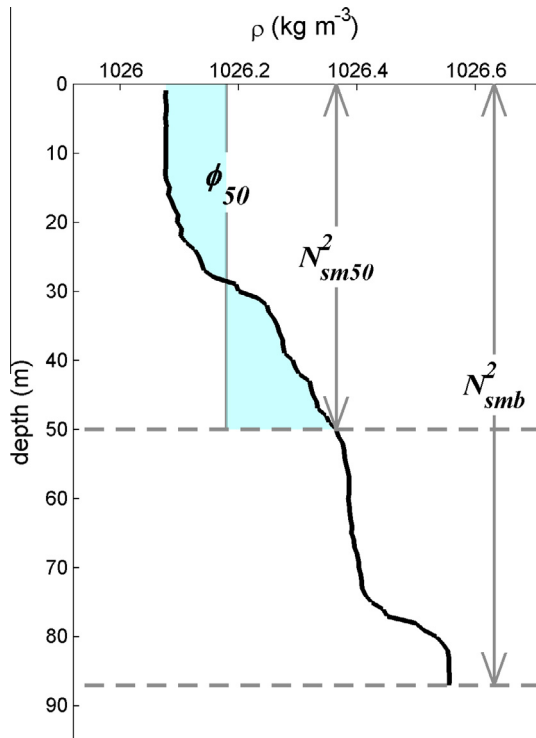


**Fig. 2.** An example of an observed density profile from April, 2010 at 69.76°W, 40.17°N. The density stratification is defined using three different criteria: surface-to-bottom Brunt–Väisälä frequency squared  $N^2_{sm6}$ , surface-to-50 m Brunt–Väisälä frequency squared  $N^2_{sm50}$ , and surface-to-50 m Simpson Energy  $\phi_{50}$  (see Section ‘Stratification criteria’ for detailed definitions).

have the greatest influence on the nutrient and phytoplankton dynamics in the upper ocean within the euphotic zone. Therefore, three different criteria of stratification are estimated in the water column. Two types of  $N^2$  are

$$N^2_{sm6} = -\frac{g}{\rho_0} \frac{\rho_s - \rho_b}{H} \quad \text{from surface to bottom} \quad (2)$$

$$N^2_{sm50} = -\frac{g}{\rho_0} \frac{\rho_s - \rho_{50}}{h_{50}} \quad \text{from surface to 50 m} \quad (3)$$

where  $\rho_0 = 1.025 \times 10^3\ kg\ m^{-3}$  is the reference density,  $H$  is the water depth (meters),  $h_{50} = \min(H, 50)$  is the depth of 50 m (if  $H > 50$  m) or sea bottom (if  $H < 50$  m),  $\rho_s$ ,  $\rho_{50}$ ,  $\rho_b$  are the densities ( $kg\ m^{-3}$ ) at sea surface, 50 m and ocean bottom, respectively; and the surface-to-50 m Simpson Energy  $\phi_{50}$  is calculated as

$$\phi_{50} = \frac{1}{h_{50}} \int_{-h_{50}}^0 (\hat{\rho} - \rho)gzdz; \quad \text{with} \quad \hat{\rho} = \frac{1}{h_{50}} \int_{-h_{50}}^0 \rho dz \quad (4)$$

Each index (2–4) was computed from the reanalysis fields and compared with the same computed directly from observations. Their representativeness was quantitatively similar (see details in Appendix), so we have chosen to focus on  $N^2_{sm50}$  in our analysis (referred to as  $N^2$  hereafter).

### Stratification climatology

Based on our assessment, the reanalysis product provides an accurate representation of the spatio-temporal patterns of density stratification across the study domain. Therefore, a stratification climatology was constructed using the 33-year assimilative hindcast as follows:

$$\text{Temporal average:} \quad \hat{N}^2(y, t) = \frac{1}{d_2 - d_1} \sum_{d=d_1}^{d_2} N^2(y, d) \quad (5)$$

$$\text{Climatological mean:} \quad \bar{N}^2(t) = \frac{1}{33} \sum_{y=1978}^{2010} \hat{N}^2(y, t) \quad (6)$$

$$\text{Standard deviation:} \quad STD(t) = \sqrt{\frac{1}{33} \sum_{y=1978}^{2010} [\hat{N}^2(y, t) - \bar{N}^2(t)]^2} \quad (7)$$

$$\text{Coefficient of variation:} \quad CV(t) = \frac{STD(t)}{\bar{N}^2(t)} \quad (8)$$

where scalar variable  $N^2(y, d)$  represents the model hindcast of stratification  $N^2$  on day  $d$  ( $1 \leq d \leq 365$ ) of year  $y$  ( $1978 \leq y \leq 2010$ ) at any given node. A 180-day low-pass filter was applied to remove intra-seasonal fluctuations prior to temporal binning of the data, and then  $N^2(y, d)$  were binned and averaged over a defined time period  $d_1 \leq d \leq d_2$  for each year to create yearly  $\hat{N}^2(y, t)$  (Eq. (5)). The representative seasonal periods are defined as: winter (January–March,  $1 \leq d \leq 90$ ), spring (April–June,  $91 \leq d \leq 181$ ), summer (July–September,  $182 \leq d \leq 273$ ) and fall (October–December  $274 \leq d \leq 365$ ). Further,  $\hat{N}^2(y, t)$  was averaged over the 33-year period to produce the climatological mean  $\bar{N}^2(t)$  as well as the associated standard deviation  $STD(t)$  and the coefficient of variation  $CV(t)$  (Eqs. (6)–(8)). For daily climatologies, Eqs. (6)–(8) were computed directly along the  $y$ -dimension of  $N^2(y, d)$ . The resulting time index  $t$  spans 365 days, 12 months and 4 seasons for daily, monthly and seasonal climatologies, respectively. For each, the mean represents the averaged strength of stratification for a given period of year, while the standard deviation provides the magnitude of interannual variations for that period, and the coefficient of variation measures the relative magnitude of

interannual variability with respect to the climatological mean, shown on a 0–100 percentile scale, with strong (weak) interannual variability approaching 100% (zero).

### Regime diagram

Because the density of seawater is primarily determined by two factors, temperature and salinity, stratification variability can be divided into thermal and haline components. Mathematically, the influence of temperature and salinity on the density of seawater is demonstrated by the equation of state,

$$\rho = \rho_0(1 - \alpha T + \beta S) \quad (9)$$

$$\alpha = -\frac{1}{\rho} \frac{\partial \rho}{\partial T}; \quad \beta = \frac{1}{\rho} \frac{\partial \rho}{\partial S} \quad (10)$$

where  $T$  and  $S$  are potential temperature ( $^{\circ}\text{C}$ ) and salinity of seawater, and  $\alpha$  and  $\beta$  are the thermal expansion ( $^{\circ}\text{C}^{-1}$ ) and saline contraction coefficients. Introducing Eq. (9) into Eq. (1) and omitting the vertical gradient of  $\alpha$  and  $\beta$  (see Gill, 1982 for a complete discussion) yields two terms,

$$N^2 = N_T^2 + N_S^2 \quad (11)$$

$$N_T^2 = g\alpha \frac{\partial T}{\partial z}; \quad N_S^2 = -g\beta \frac{\partial S}{\partial z} \quad (12)$$

where  $N_T^2$  and  $N_S^2$  are the thermal and haline components ( $\text{s}^{-2}$ ) of  $N^2$ , respectively (this also applies to Eqs. (2) and (3)). The establishment of stratification depends on the net effects of thermal and haline controls. The relative importance of the two components can be gauged using their ratio  $\gamma$ , which is computed as

$$\gamma = -\frac{\alpha \partial T / \partial z}{\beta \partial S / \partial z} \quad (13)$$

By considering two water properties vertically separated by  $\Delta z$ , with the corresponding temperature and salinity differences equal to  $\Delta T$  and  $\Delta S$ , respectively, Eq. (13) can be approximated as

$$\gamma \approx -\frac{\alpha \Delta T}{\beta \Delta S} \quad (14)$$

The ratio  $\gamma$  depends upon two parameters  $-\frac{\alpha}{\beta}$  and  $\frac{\Delta T}{\Delta S}$ . Interpreted in the conventional temperature–salinity ( $T$ – $S$ ) diagram,  $\frac{\Delta T}{\Delta S}$  represents the slope of a  $T$ – $S$  curve defined by two water masses that stratify the water column, while  $-\frac{\alpha}{\beta}$  measures the slope of the normal vector to the density contour through any given point  $\rho(S, T)$  (Fig. 3a). Despite the fact that  $-\frac{\alpha}{\beta}$  is influenced by both temperature and salinity, water temperature is the predominant contributor. In a more general sense,  $-\frac{\alpha}{\beta}$  is a state parameter that can be directly derived from  $T$  and  $S$ , representing the ability of the water column to expand/shrink, whereas  $\frac{\Delta T}{\Delta S}$  reflects the ratio of vertical temperature and salinity differences. It should be noted that many combinations of two slopes give the same  $\gamma$ , suggesting the possibility of transition among different regimes.

Using  $-\frac{\alpha}{\beta}$  and  $\frac{\Delta T}{\Delta S}$  as two axes, a  $\gamma$ -diagram is constructed describing the parameter space. In order to maintain a positive horizontal axis, we move the minus sign from  $-\frac{\alpha}{\beta}$  to  $\frac{\Delta T}{\Delta S}$ . Lines of constant  $\gamma$  are shown as curved contours (Fig. 3b). The contours of  $|\gamma| = 1$  divide the parameter space into two regimes:  $|\gamma| > 1$  suggests thermal controls are dominant over haline controls in density stratification ( $|N_T^2| > |N_S^2|$ ), while  $|\gamma| < 1$  suggests that haline controls are dominant ( $|N_T^2| < |N_S^2|$ ). It should be noted that the isopleths of  $\gamma$  converge toward the positive direction of the horizontal axis, such that the blue zone in Fig. 3b narrows at high values of  $\frac{\Delta T}{\Delta S}$ . This

suggests that a water mass having high  $\frac{\Delta T}{\Delta S}$  is more prone to  $|\gamma| > 1$  regimes (thermally dominant) and more sensitive to changes in  $\frac{\Delta T}{\Delta S}$ . Therefore, the  $\gamma$ -diagram provides a convenient way to identify the stratification regime (e.g., under contrasting conditions, such as cold versus warm water, or warming versus cooling events, or freshening versus salinification events).

## Results

### Seasonal evolution of $N^2$

The stratification climatology exhibits a strong seasonal cycle on the Northwest Atlantic continental shelf and in the GoM region (Fig. 4). In winter,  $N^2$  is weak ( $< 1 \times 10^{-4} \text{ s}^{-2}$ ) over the shelf and in the GoM but slightly higher ( $\sim 2 \times 10^{-4} \text{ s}^{-2}$ ) near the shelf-slope front (Fig. 4a). The water column in the WGoM is strongly mixed consistent with observations of wintertime convection in this area (Taylor and Mountain, 2009). In spring, the stratification increases throughout the region, exceeding  $2 \times 10^{-4} \text{ s}^{-2}$  on the MAB and  $1 \times 10^{-4} \text{ s}^{-2}$  in the GoM and NSS regions (Fig. 4b). During summer, the stratification hits its annual peak everywhere, yet regional differences are prominent, with  $> 6 \times 10^{-4} \text{ s}^{-2}$  in the SMAB,  $4\text{--}6 \times 10^{-4} \text{ s}^{-2}$  in the NMAB, WGoM and NSS regions and  $3\text{--}4 \times 10^{-4} \text{ s}^{-2}$  in the EGoM (Fig. 4c). The stratification breaks down quickly during fall, dropping below  $1 \times 10^{-4} \text{ s}^{-2}$  on the MAB and in the GoM, approaching winter levels, while it continues to decay on the NSS and near the shelf-slope front (Fig. 4d).

The seasonal evolution of stratification  $STD$  over the 33-year period follows a pattern that is similar to the climatological mean, increasing at the beginning of the year, peaking in summer and decreasing in fall (Fig. 4e–h). In addition, the regional differences in  $STD$  resemble that of  $N^2$ , with high  $STD$  occurring in regions of high  $N^2$ . The overall range of  $STD$  is one-order of magnitude smaller than that of  $N^2$ , suggesting interannual variations do not exceed the seasonal variation in most areas. Despite weaker stratification during fall–winter, the results show high  $CV$  ( $> 30\%$ ) at those times of year, in comparison to low ( $< 20\%$ ) during summer (Fig. 4i–l). Spatially, most areas in the GoM and GB, on the inner shelf of the MAB and along the coasts of the NSS exceed 90%  $CV$  during wintertime, indicating that the year-to-year variation of the strength of winter stratification is comparable to the mean in these regions, suggestive of changes in stratification timing.

Spatial differences at regional level are further examined using the daily climatologies for each of the five subregions (see Fig. 1 for location). The time series from all subregions shows a similar annual curve that peaks once a year between late July and early August, and remains stratified above  $1 \times 10^{-4} \text{ s}^{-2}$  for 6–8 months (Fig. 5a). However, the timing of peak stratification clearly shows a northward progression, occurring roughly half of one month earlier in the SMAB than the NSS region. The magnitude and  $STD$  are strongest in the SMAB and weakest in the EGoM among the five subregions, with the peak  $N^2$  being generally stronger on the shelf (MAB and NSS) than in the GoM. While the timing of the annual cycle is similar in the western and eastern GoM, the WGoM exhibits a larger annual range. These differences are consistent with those inferred from the 10-year MARMAP dataset (Mountain and Manning, 1994). The finer spatial structures will be discussed in more detail in the following sections.

### Thermal versus haline controls

The density stratification  $N^2$  consists of two components,  $N_T^2$  and  $N_S^2$ , which may vary in their response to different forcings. As such, it is expected that  $N_T^2$  and  $N_S^2$  vary over a seasonal cycle and

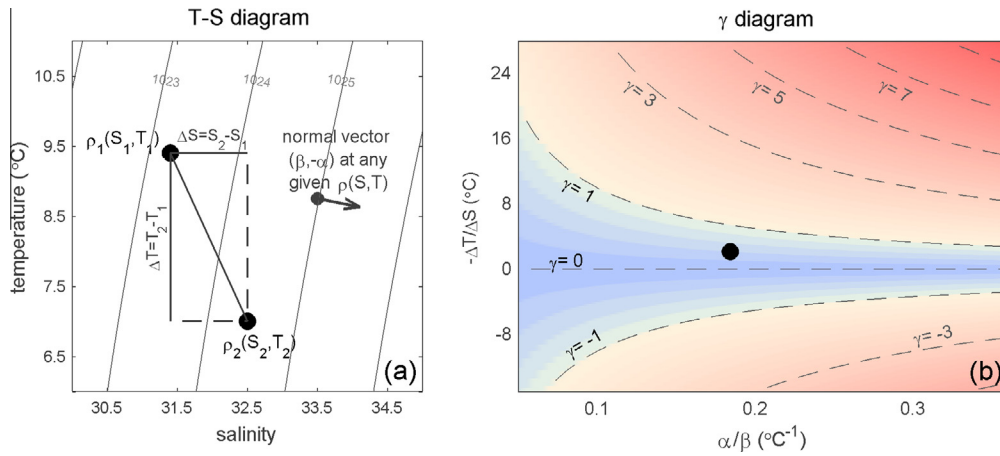


**Fig. 3.** An example of (a) temperature–salinity (T–S) diagram and (b) its corresponding  $\gamma$ -diagram. The  $\gamma$ -diagram is used to classify the relative importance of thermal versus haline controls on the density stratification. The two parameters that form the axes of  $\gamma$ -diagram are delineated in the T–S diagram:  $\Delta T/\Delta S$  represents the slope of the T–S curve defined by two water masses  $\rho_1(S_1, T_1)$  and  $\rho_2(S_2, T_2)$  that stratify the water column, while  $-\alpha/\beta$  measures the slope of the normal vector to the density contour through any given point  $\rho(S, T)$ . In the  $\gamma$  diagram,  $-1 < \gamma < 1$  indicates that haline control  $N_S^2$  is dominant (blue zone), while  $|\gamma| > 1$  indicates that thermal control  $N_T^2$  is dominant (red zones). (For interpretation of the references to color in this figure legend, the reader is referred to the web version of this article.)

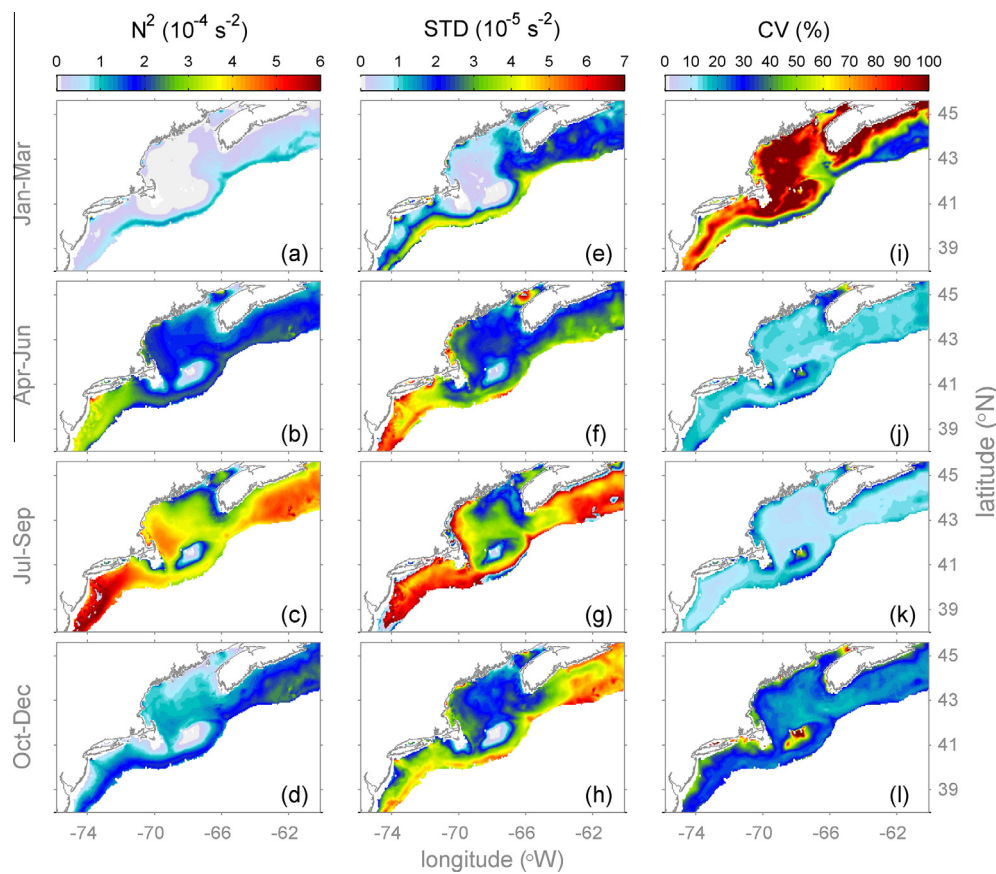


**Fig. 4.** The spatial patterns of (a)–(d) seasonal stratification climatology  $N_{sm50}^2$ , (e)–(h) its standard deviation (STD) and (i)–(l) coefficient of variation (CV) on the Northwest Atlantic shelf. In subpanels (a)–(d), the regions with extremely weak stratification ( $< 10^{-5} \text{ s}^{-2}$ ) are marked in light gray.

that their magnitude and timing may differ in such a way that their interplay reinforces and/or compensates the other. For this reason, it is instructive to examine the components separately in order to quantify their relative importance in determining the density stratification both temporally and spatially.

The regional averages of  $N_T^2$  display an annual cycle that is similar to  $N^2$  (Fig. 5b), that is,  $N_T^2$  peaks once a year and the peak timing propagates northward, coinciding with the seasonal evolution of surface heating. Specifically,  $N_T^2$  peaks earliest in the SMAB (late

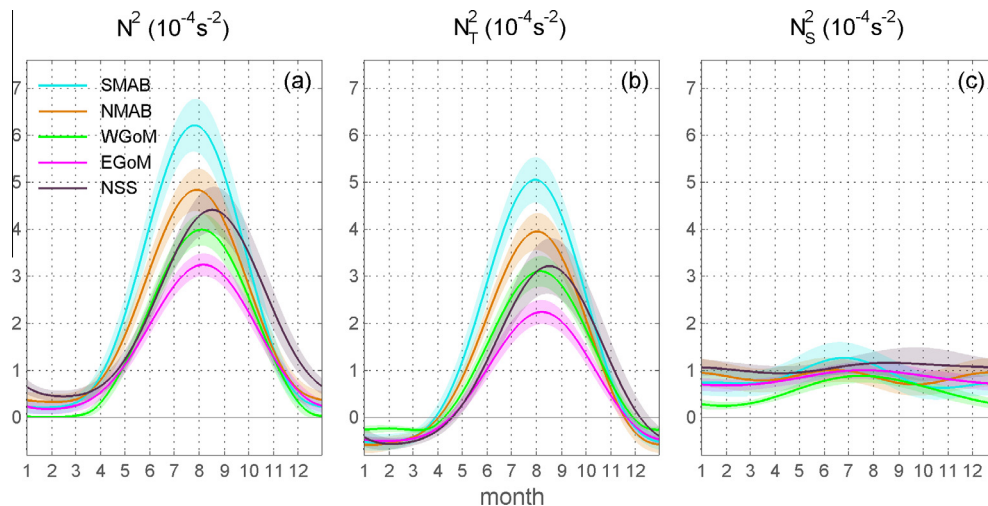


**Fig. 5.** Time series of climatological daily stratification, in the five subregions as specified in Fig. 1. Three subpanels show the (a) total, (b) thermal and (c) haline stratification, with the shaded areas representing their respective standard deviation over the period 1978–2010.

July) and latest in the NSS (mid-August). Also, the peak magnitude of  $N_T^2$  is stronger on the shelf than in the GoM regions, with the strongest ( $\sim 5 \times 10^{-4} \text{ s}^{-2}$ ) in the SMAB and the weakest in the EGoM ( $\sim 2 \times 10^{-4} \text{ s}^{-2}$ ). A unique feature of  $N_T^2$  is the sustained period of negative values from November to May, suggesting cold water overlying warm water. If uncompensated by haline controls, the effect on the overall stratification will lead to overturning in the water column. In addition, the *STD* of the climatological  $N_T^2$  displays clear regional and temporal differences (Fig. 5b), showing larger ranges in summer months than the rest of the year, and in the shelf region than in the GoM region.

Compared with  $N_T^2$ , the regional averages of  $N_S^2$  display relatively weak annual variations (ranging from  $0.2\text{--}1.5 \times 10^{-4} \text{ s}^{-2}$ ) and region-dependent seasonality (Fig. 5c). In the NMAB,  $N_S^2$  peaks twice per year. The first peak occurs in late July, related to the increase in the Hudson River discharge which peaks in spring (April–May, c.f., Castelao et al., 2008). The second peak occurs in late November with a short-lived destratified period between the two peaks. The second peak may be a result of the interaction between seasonal wind forcing and the haline influence of the shelf-slope front. While strong winds induce vertical mixing that erodes stratification in the early fall, the cross-shelf flow induced by persistent alongshore winds also displaces the saltier shelf-slope front onshore, thereby enhancing haline stratification over the mid-shelf during winter (Lentz et al., 2003). In the WGoM and EGoM,  $N_S^2$  peaks just once per year, in mid-July. The peak in the EGoM lags the peak of local river discharge (usually in May of previous year) by roughly 9–10 months (c.f., RIVSUM index, (Smith, 1989)), while stratification in the WGoM lags local river discharge by 0–1 months (c.f., Mountain and Manning, 1994).  $N_S^2$  in the EGoM exceeds that in the WGoM throughout the year, implicating the importance of fresher inflow from the NSS (Smith, 1989).  $N_S^2$  in the NSS region is considerably less variable, remaining near  $1 \times 10^{-4} \text{ s}^{-2}$  throughout the year, despite a slight increase from July to September. The *STD* of  $N_S^2$  shows large spatial differences, with larger ranges on the shelf than in the GoM. In each sub-region, seasonal variations of *STD* are not evident.

The variations in  $N_T^2$  and  $N_S^2$  suggest that their relative contribution to the overall stratification varies both seasonally and regionally. This is clearly illustrated by the seasonal changes in the magnitude and distribution of  $\gamma$  (Fig. 6, see Section ‘Regime

diagram’ for the definition of  $\gamma$ ). During winter,  $\gamma$  is negative throughout the domain, ranging from  $-1$  to  $0$  (Fig. 6a), suggesting that  $N_T^2$  and  $N_S^2$  are comparable yet compensating. Changes in  $N_T^2$  at this time of year are dominated by atmospheric cooling, while ocean advection maintains  $N_S^2$ . During spring,  $\gamma$  becomes positive (Fig. 6b), suggesting that the two components work together to build stratification in the upper water column. While  $\gamma$  is still below 1 (weaker  $N_T^2$ ) in the EGoM, the offshore NSS and shelf-slope front regions,  $\gamma$  slightly exceeds 1 in the MAB, WGoM and near-shore NSS regions. During summer,  $N_T^2$  is the predominant component everywhere in the study area, with  $\gamma$  ranging from 1 to above 7 (Fig. 6c), consistent with patterns shown by the time series analysis (Fig. 5b and c). During fall (Fig. 6d),  $\gamma$  drops below 1 reflective of the reduction in  $N_T^2$  to levels comparable with  $N_S^2$ . In general,  $N_S^2$  becomes more important during cooler months while  $N_T^2$  dominates during warmer months. The entire domain spends some time in the negative  $\gamma$  regime. By comparison, the MAB and nearshore NSS exhibit stronger and longer thermal control (about 6 months). Overall, except in summer,  $N_T^2$  and  $N_S^2$  are both important in determining the density stratification over an annual cycle.

#### Timing and magnitude

The daily stratification climatology allows us to examine the regional phenology of stratification, quantifying the timing of key transition points that may have biological implications. Except in the vicinity of the shelf-slope front, the annual peak in stratification occurs progressively later from south to north across the region (Fig. 7a), peaking earliest in the MAB region (late-July), followed by the GoM region (early August) and finally in the NSS region (mid-to-late August). On the shelf, the progression of peak timing is offshore in the MAB but inshore in the NSS region, a pattern largely associated with advective processes. In the MAB, thermal stratification is progressively enhanced by low-salinity water that spreads from major river plumes that are driven offshore by upwelling-favorable (eastward) wind stresses (Lentz et al., 2003). The shoreward progression on the NSS is a consequence of cold-water advection by a coastal jet on the inner shelf (though the salinity is low), where the advective cooling postpones the peak of  $N^2$ . The peak magnitude is higher in the MAB and outer NSS ( $>6 \times 10^{-4} \text{ s}^{-2}$ ), but lower in the GoM and nearshore region of NSS ( $<5 \times 10^{-4} \text{ s}^{-2}$ ) (Fig. 7b), a pattern likely due to receiving cold

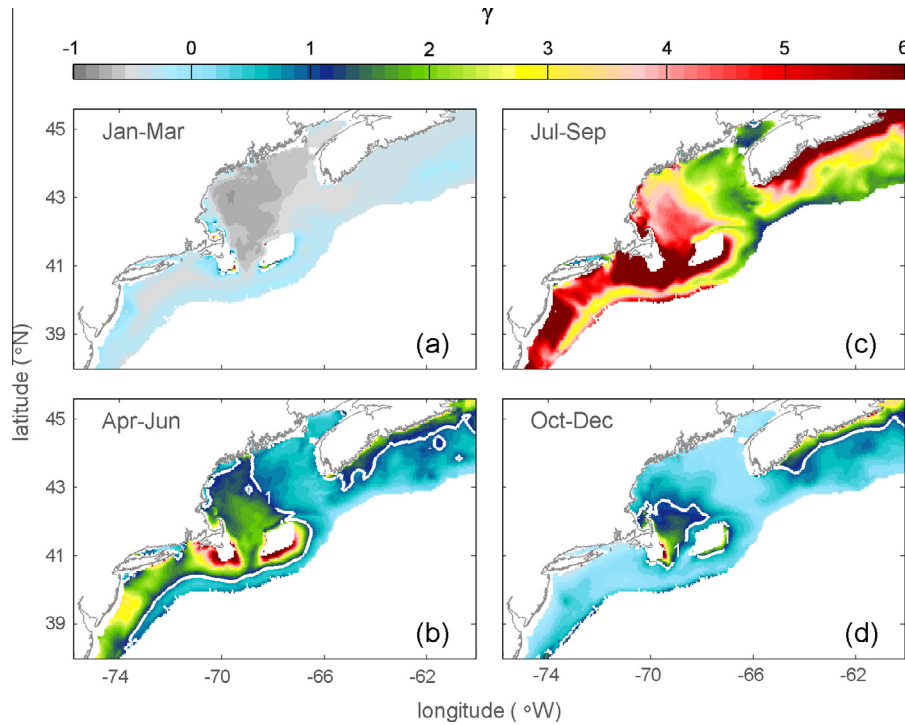


**Fig. 6.** The spatial distribution of seasonal  $\gamma$  (the ratio between  $N_T^2$  and  $N_S^2$ , see Section ‘Regime diagram’ for details) on the Northwest Atlantic shelf. The white contour represents  $\gamma = 1$  where  $N_T^2$  and  $N_S^2$  are of equal importance in determining the surface-to-50 m density stratification.

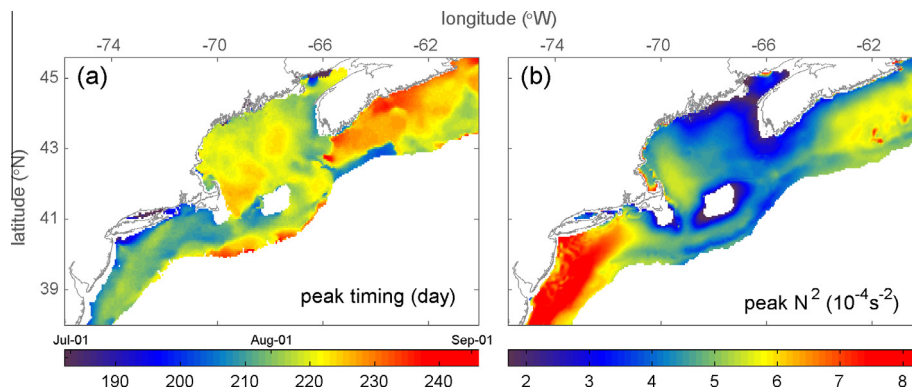


**Fig. 7.** The spatial pattern of the (a) timing and (b) magnitude of peak stratification on the Northwest Atlantic shelf based on the surface-to-50 m stratification climatology.

inflows from higher latitude (e. g., [Smith, 1989](#)) and/or strong tidal mixing in those regions (e.g., [Brooks and Townsend, 1989](#)).

The interaction between thermal and haline effects points to key transitions in the system ([Fig. 8](#)). Throughout the annual cycle,  $N_S^2$  remains weak but positive, always contributing to the stabilization of the water column. In contrast,  $N_T^2$  exhibits a much larger annual range, spanning weakly negative to strongly positive values. During periods when  $N_T^2$  is negative, it is acting against the stabilizing effect of  $N_S^2$ . As  $N^2$  builds in winter–spring,  $N_T^2$  transitions from a negative state, associated with surface cooling, convection and vertical mixing, to a positive state, associated with surface heating and the re-establishment of  $N_T^2$ . As  $N_T^2$  continues to build, the system becomes thermally dominant, as marked by the point when  $N_T^2$  exceeds  $N_S^2$ . On the other side of the annual peak, as  $N^2$

ramps down,  $N_T^2$  weakens to the point where haline control dominates,  $N_T^2 < N_S^2$ , before finally becoming negative again. Based on this progression, we identify two metrics that are useful for marking the beginning and end of important phases in the development and breakdown of stratification,  $N_T^2 = 0$  and  $N_T^2 = N_S^2$ .

During the course of stratification development,  $N_T^2 = 0$  marks the beginning of the development of a seasonal thermocline. In general, this phase occurs between early March and late May across the Northwest Atlantic shelf ([Fig. 9a](#)). There is a clear latitudinal shift in the time at which  $N_T^2 = 0$  across the region, with earlier transition in the MAB and later on the NSS, following the phase of atmospheric heating across the region ([Bunker, 1976](#); [Umoh et al., 1995](#)). A noteworthy feature of the spatial pattern is the strong cross-shelf gradient (i.e., from inner shelf to shelf-slope front), where shallow regions hugging the shoreline tend to show

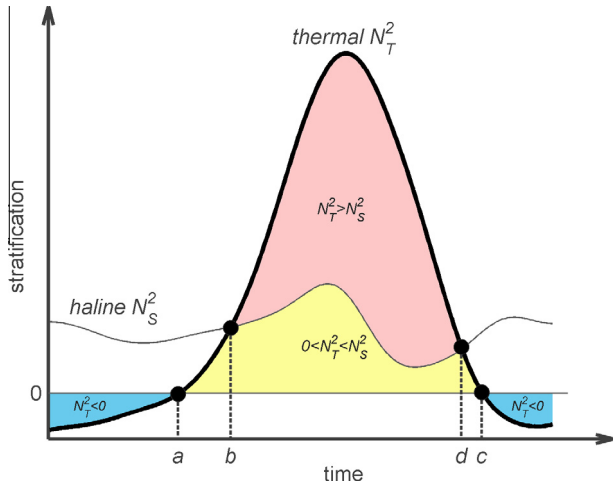


**Fig. 8.** A conceptual plot of annual curves of thermal ( $N_T^2$ ) and haline ( $N_S^2$ ) stratification. Owing to their interaction, four key transition points that define the beginning/end of thermally-positive ( $N_T^2 > 0$ ) and thermally-dominant ( $N_T^2 > N_S^2$ ) states are identified and marked in labels corresponding to the panels in Fig. 9.

shutdown of convection earlier than deeper regions away from the coast. This is consistent with in-situ observations collected by glider across the shelf in the southern MAB (Castelao et al., 2010). Interestingly, the  $N_T^2 = 0$  timing appears to coincide with the timing of the winter–spring bloom over most of the study region (cf., Song et al., 2010).

During the development of stratification, when  $N_T^2$  enters its positive phase,  $N_T^2 = N_S^2$  marks the transition from a haline dominated regime to a thermally dominated regime (Fig. 9b). The timing ranges from mid-April to late-June over most of the region, with the earliest transition occurring in the MAB, WGoM and near-shore NSS regions and later transition following in the EGoM and offshore NSS regions. Not surprisingly, the pattern resembles the April–June  $\gamma$ -ratio distributions (Fig. 6b) since the timing considers the interplay between  $N_T^2$  and  $N_S^2$ . A region with relatively strong

haline control, like the EGoM where fresh source waters first enter the GoM or at the shelf edge in the vicinity of the shelf-slope front, will postpone the development of the thermally-dominant state.

During late-summer/early-fall, the system transitions out of the thermally dominated regime as atmospheric cooling and wind-induced mixing erode thermal stratification. The transition occurs between mid-September and late-November, as indicated by Fig. 9d, largely mirroring the development phase, with water-column warming occurring faster inshore in the MAB and offshore on the NSS. The pattern on the NSS suggests that the advection of low-salinity water from higher latitude into those regions plays an important role in promoting the termination of thermally-dominant control. Finally, the stratification breakdown phase culminates when  $N_T^2 = 0$ , generally in early November to December, with early (late) breakdown in the southern (northern) regions (Fig. 9c).

**Discussion**

*Different regimes of thermal versus haline control*

In the study region, the interaction between thermal and haline control may result in distinct annual regimes, which have not been fully demonstrated in previous studies, yet can be clarified using the  $\gamma$ -diagram (see Section ‘Regime diagram’ for details). For the five subregions, monthly mean values of the two key parameters  $\frac{\alpha}{\beta}$  and  $-\frac{\Delta T}{\Delta S}$ , as well as their individual parameters, are computed from the daily climatology. The seasonal change in  $\alpha$  is much larger than the change in  $\beta$ , suggesting that temperature dominates  $\frac{\alpha}{\beta}$  (Fig. 10a–c). The phase difference between  $-\frac{\Delta T}{\Delta S}$  and  $\frac{\alpha}{\beta}$  (Fig. 10c and f) cause the annual curves in the  $\gamma$ -diagram to rotate clockwise, reflecting the increasing importance of thermal (haline) control during warmer (cooler) months (Fig. 11). In the winter–spring season, all subregions spend some time in the negative  $\gamma$ -regime, when the water column is thermally destratified but compensated by haline controls. The evolution is consistent with the spatio-temporal patterns shown in Figs. 5 and 6. In addition, all of the curves stay above the  $\gamma = 1$  isopleth for several months, suggesting the

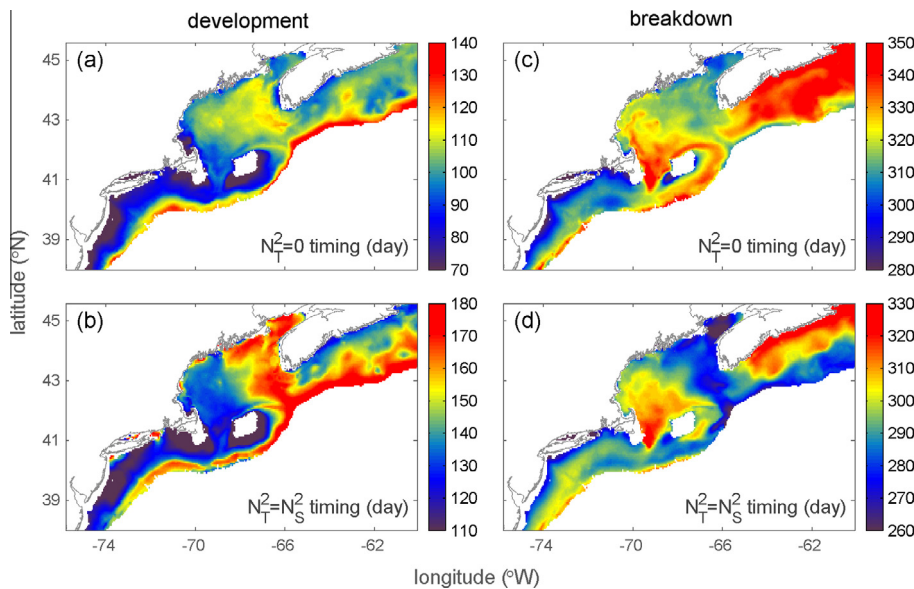


**Fig. 9.** The spatial pattern of the timing associated with (a/c)  $N_T^2 = 0$  and (b/d)  $N_T^2 = N_S^2$  during the course of the annual stratification development and breakdown on the Northwest Atlantic shelf. The daily climatology of surface-to-50 m stratification is used. At any location, the timing goes from (a), (b), (d) to (c) throughout the annual cycle (see Fig. 8).

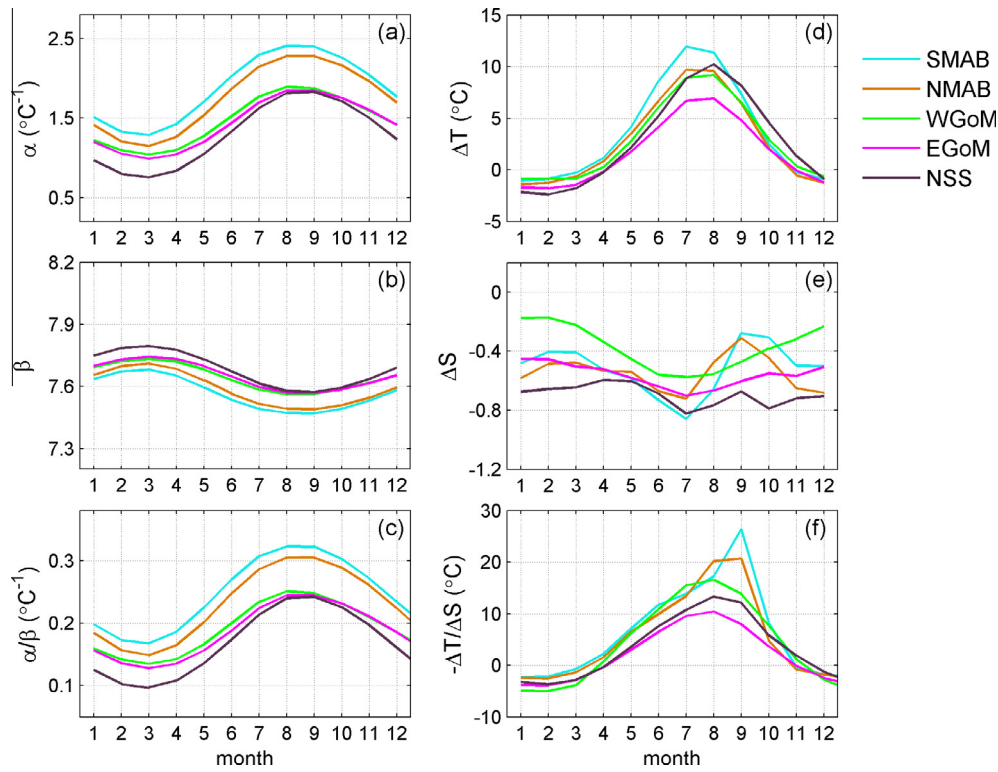


**Fig. 10.** Time series of key parameters used in the  $\gamma$ -diagram for the five subregions as specified in Fig. 1.

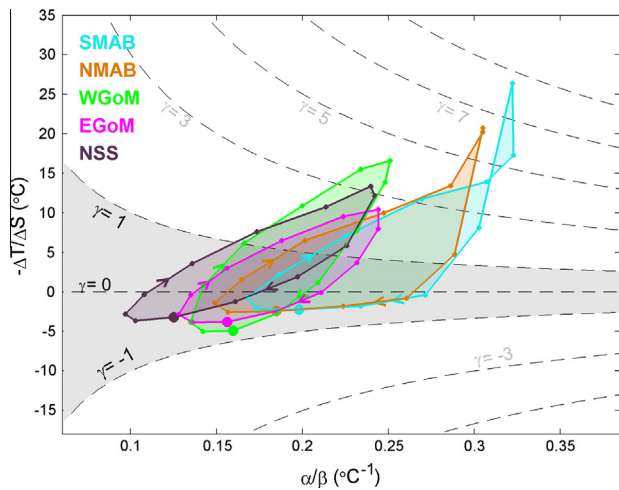


**Fig. 11.** Regime diagram of the annual cycle of stratification in the five subregions specified in Fig. 1. The horizontal axis  $\alpha/\beta$  represents the ratio between thermal and haline coefficients; the vertical axis  $-\Delta T/\Delta S$  represents the ratio between surface-to-50 m temperature and salinity gradients (see details in Section ‘Regime diagram’). The gray and white zones delineate regimes dominated by haline and thermal controls, respectively. Each dot represents the monthly mean computed using the daily climatology, with January conditions marked by a large dot. The annual cycles rotate clockwise as indicated by the arrows.

dominance of thermal controls during the warmer period of the year.

Despite the similarities, several notable regional differences exist: (1) the MAB curves are centered farther right in the regime diagram, display the strongest  $\frac{\alpha}{\beta}$ , and remain within the thermally-dominant regime for the greatest portion of the year, while the opposite is true for the NSS curve; (2) the MAB regions feature the widest range of  $\frac{\Delta T}{\Delta S}$  over a year, exhibiting the strongest seasonal

variation. In comparison, the NSS and EGoM regions exhibit weak variations in  $\frac{\Delta T}{\Delta S}$ ; (3) the MAB region has a stronger ( $\gamma > 5$ ) and longer ( $> 6$  months) thermally dominant phase than the other regions; (4) the WGoM has the lowest  $\gamma$ -values, suggesting that the water column tends to be strongly mixed during winter; (5) the latitudinal progression of transitions during the development phase is northward, as shown by the intersection of the  $\gamma = 0$  and  $\gamma = 1$  isopleths by the annual curves. The caveat is that the regional averages mask spatial variances across the shelf, so the differences are indicative of broader heterogeneity along the shelf.

#### What drives the spatio-temporal patterns

The overall stratification pattern suggests a latitudinal organization to the regimes (Fig. 11). Specifically, the seasonal cycle of stratification is marked by strong thermal control in the southern subregions, whereas haline effects become more important in the regions to the north. This pattern is likely a joint consequence of the southward increase in average water temperatures and decrease in freshwater transport, as warmer water temperatures yield larger  $\frac{\alpha}{\beta}$  (Fig. 3a) and saltier water contributes to weaker  $\Delta S$ . Water temperatures are warmer in southern subregions, due to strong atmospheric heating, the active exchange with neighboring warm slope water, and the absence of direct cold water input from higher latitudes. This is particularly true in contrast to the NSS and EGoM regions, which receive colder and fresher inflows directly from higher latitudes and weaker surface heating throughout the year (Loder et al., 1998). This latitudinal organization does not necessarily apply to the nearshore and shelf-slope front regions, where subsurface advection of both temperature (e.g., cold intermediate layer) and salinity (slope water intrusions) can complicate the picture.

There is also a clear temporal organization to the regimes over the seasonal cycle (Fig. 11). For instance, haline effects dominate

over thermal effects in density stratification from October through late April (Fig. 6). While it has long been recognized that surface heating is the dominant agent driving the seasonal cycle of stratification in the upper water column (Beardsley et al., 1985; Smith, 1989; Mountain and Manning, 1994), this seems an oversimplification during winter–spring. Our analysis suggests that, even though vertical temperature gradients can be diminished through winter cooling (e.g., Taylor and Mountain, 2009; Castelao et al., 2010), vertical salinity gradients can persist through the advection of low-salinity water, for instance, the spread of buoyant river plumes (e.g., Zhang et al., 2009), the transport of coastal jets (e.g., Loder et al., 2003), the wind-induced downwelling or the onshore movement of shelf-slope fronts (e.g., Lentz et al., 2003). Nevertheless, the variability during the haline dominated period is pronounced around the climatological mean (compare Figs. 4 and 6), indicating the existence of significant interannual variability. A more comprehensive understanding of the processes that govern the winter–spring haline stratification is clearly needed.

Regional differences have been noted in previous studies, yet the spatial and temporal scales associated with these features remain unclear due to the resolution of observations. A high-resolution reanalysis product is able to bridge the gap between knowledge derived from non-uniform observations and the spatio-temporal scales needed. For example, using sustained glider observations, Castelao et al. (2010) reported that, unlike the northern MAB near Nantucket Shoals (Beardsley et al., 1985; Lentz et al., 2003), the stratification climatology in the central MAB off New Jersey is marked by large seasonal variations in surface salinity induced by Hudson outflow. By taking advantage of the high-resolution stratification climatology we have confirmed this difference by resolving a transition between strong and weak thermal control from Nantucket Shoals to the Hudson Valley Shelf (Fig. 6). Similarly, Mountain and Manning (1994) created statistically extrapolated maps of 52 standard stations repeatedly occupied 3–6 times per year over the period 1977–1987, and found west–east stratification asymmetry in the GoM. Our Figs. 5 and 6 clearly show a difference between the western and eastern GoM in nearly all seasons. Previous studies have attributed the asymmetry to a number of factors, such as the Saint John River inflow, the Maine coastal current, and enhanced wintertime convection in parts of the WGoM (e.g., Mountain and Manning, 1994; Taylor and Mountain, 2009). From the perspective of thermal versus haline controls on stratification, thermal control is more pronounced in the west than in the east, leading to larger amplitude seasonal variations (Figs. 5 and 11). Our results corroborate their results and provide additional details regarding timing and magnitude.

#### *Implications for ecosystem dynamics*

The climatology is produced within some envelope of interannual variability. As shown by the high CVs despite low *STDs* (Fig. 4i–l), winter–spring stratification in the MAB and GoM regions varies from year to year. The evolution of nutrient distributions and related marine primary productivity in subsequent seasons can be strongly influenced by these interannual changes (e.g., Ji et al., 2007; Xu et al., 2011). Since seasonal fluctuations dominate the hydrographic variability over most of the study area, our seasonal climatology provides the framework necessary for evaluating interannual changes. A detailed analysis of interannual variability using this long-term high-resolution reanalysis product is beyond the scope of this study.

We have identified indices related to the phenology of stratification that should be useful for understanding and predicting the biological response to physical drivers. For instance, both in situ and satellite-derived chlorophyll observations are gappy and lead to uncertainties in bloom timing estimation (e.g., Siegel et al.,

2002; Yamada and Ishizaka, 2006; Sharples et al., 2006; Brody et al., 2013). The high-resolution indices developed in this study are valuable and can be used to track the timing of convection shutdown in the upper water column and the consequent increase in surface chlorophyll concentrations (cf. Ferrari et al., 2014 in the subpolar North Atlantic). Similarly, the indices of destratification timing can be used to infer alleviation of nutrient- or light-limitation conditions (Xu et al., 2011). In a changing climate, a clear understanding of the phenology of stratification on relevant spatial scales can benefit the prediction of year to year changes in bloom timing and spring productivity (Ji et al., 2007, 2008; Song et al., 2010, 2011).

Characterizing spatio-temporal distributions of stratification is critical to synthesizing existing data and modeling efforts in support of ecosystem assessments for the Northeast US Continental Shelf Large Marine Ecosystem. For instance, in the MAB region, previous studies suggest that fall bottom temperature is influenced by fall destratification (Mountain and Holzwarth, 1989), and can be linked to surf clam distributions (Weinberg, 2005) as well as the nursery habitats of young-of-the-year yellow tail flounder (Sullivan et al., 2005). With the stratification reanalysis developed here, immediate examination of the link is warranted. In the absence of long-term and high-resolution observations, the stratification indices, in combination with historical fishery data, also provide a plausible approach to assess the hypothetical linkages between water-column stability and recruitment variability in fish populations. For instance, fluctuations in stratification could affect the success of larval feeding, change the timing and productivity of plankton, and modify community structure (e.g., stable ocean hypothesis (Lasker and Zweifel, 1978), optimal window hypothesis (Cury and Roy, 1989), match-mismatch hypothesis (Cushing, 1990)). As climate-related warming and freshening continue to affect water column stability, understanding the changing stratification is a critical first step in anticipating the potential impact on larval recruitment.

#### **Summary**

A long-term high-resolution reanalysis of hydrographic fields was developed based on NECOFS for the Northwest Atlantic shelf region. Using this product, a spatio-temporally explicit stratification climatology was constructed to examine the distribution and timing of seasonal stratification. The periodic nature of atmospheric heating/cooling acting on the region and the advective influence of local and remote sources drive a strong interplay between thermal and haline controls, leading to distinct regional patterns. A  $\gamma$ -diagram was developed to distinguish stratification regimes based on the temporal evolution of stratification and its thermal and haline controls. The diagram highlights clear transitions along latitudinal extent and throughout the seasonal cycle – the MAB region being generally dominated by thermal control through most of the year, while haline control is more important in the NSS–EGoM regions. The winter–spring stratification is more sensitive to haline effects, which may explain some interannual changes in nutrient conditions, marine primary productivity and high-level consumers.

#### **Acknowledgements**

This work was supported by NOAA's Fisheries and the Environment Program, Grant #12-03 and through NOAA Cooperative Agreement NA09OAR4320129. RJ worked on this paper as a CINAR (Cooperative Institute for the North Atlantic Region) Fellow. The authors would like to thank three anonymous reviewers and the editor for their valuable comments.

## Appendix

In our study, we use the data-assimilative high-resolution reanalysis database that was created through hindcast NECOFS experiments (<http://porpoise1.smast.umassd.edu:8080/fvcomwms/>). The reanalysis can be regarded as gap-filling, using a model that utilizes ocean dynamics to constrain the interpolation. In other words, the model runs forward in time to simulate the ocean state independent of observations, and then the simulated fields are corrected by observations when and where available. The second step is designed to reduce model uncertainties resulting from external forcing, parameterizations, and discretization, making the use of existing observations essentially valuable. The hydrodynamics model in NECOFS is the third generation of GoM-FVCOM with a computational domain encompassing the shelf region between 35 and 46°N in the Northwest Atlantic ocean (Fig. A1c), with a horizontal resolution ranging from ~0.3–1.0 km near the coast to a maximum of ~10–20 km near the outer boundary. Vertically, FVCOM employs a hybrid coordinate derived from a generalized terrain-following coordinate (Chen et al., 2013), allowing for improved simulation of stratification and mixing within the boundary layers. A Smagorinsky formulation (Smagorinsky, 1963) is used to parameterize horizontal diffusion and turbulent vertical mixing is calculated using the General Ocean Turbulence Model (GOTM) libraries (Burchard, 2002), with the 2.5 level Mellor-Yamada (Mellor and Yamada, 1982) turbulence model used as the default. Additional adjustment was conducted to bring about immediate overturn when the water column becomes unstable. The model is forced by wind stress, surface net heat flux and net P-E at the air–sea interface, by local river runoff at the coast, and by tides at the open boundary with temperature, salinity and flow specified through nesting to a Global version of FVCOM. The

surface forcing fields were computed using the NCEP/NCAR WRF model configured for the region (9-km resolution) and the COARE3 bulk air–sea flux algorithm (Chen et al., 2005). The assimilated observation dataset consisted primarily of satellite-derived SST, temperature and salinity profile data whose distribution was concentrated along shipping routes and historically occupied stations. It incorporates almost all observational data that is available in the model domain, including observations from US and Canadian databases, open-access sources and via individual PI's (animation available from [http://delmar.whoi.edu:8080/thredds/fileServer/testAll/2013\\_FATE\\_Stratification/gom\\_ts\\_xy\\_1978-2010.gif](http://delmar.whoi.edu:8080/thredds/fileServer/testAll/2013_FATE_Stratification/gom_ts_xy_1978-2010.gif)). The assimilation was conducted regionally using optimal interpolation based on spatio-temporal scales determined from covariance analysis. The resulting ocean reanalysis provides daily estimates of four-dimensional hydrographic fields spanning the period 1978–2010, an improvement over estimates based solely on numerical simulation or sparse observations that allows us, even in relatively data-sparse areas, to estimate the evolution of the hydrographic properties over synoptic, seasonal and interannual time scales.

Despite the fact that stratification is influenced by three-dimensional processes, most of the seasonal stratification variability in this region is concentrated in the upper 50 m. Seasonally, the observed surface mixed layer depth (calculated as  $0.125 \text{ kg m}^{-3}$  relative to density near the sea surface, a method used by Boss and Behrenfeld (2010)) is less than 50 m at most locations (68% of total profiles in observations). At four representative cross-sections in different subregions, the spectral power of stratification within the seasonal band is strongest in the upper 50 m of the water column and decreases with depth (Fig. A2). This allows us to focus on the upper 50 m of the water column, assuming that the surface layer stratification will have the greatest influence on the nutrient and phytoplankton dynamics in the upper ocean

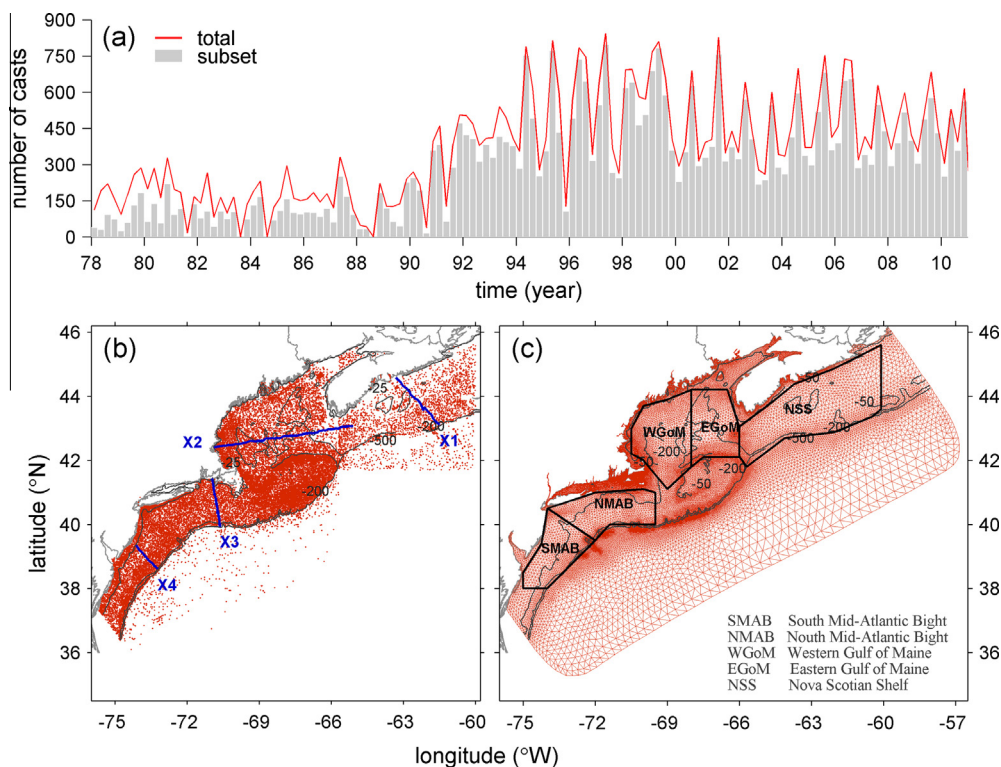


**Fig. A1.** (a) The number of in situ temperature and salinity profiles collected over the period 1978–2010 on the Northwest Atlantic shelf, with total casts shown in red and the subset used in this analysis depicted by the gray histogram. (b) The geographic distribution of all 48,243 profiles and locations of 4 cross-shelf sections in Fig. A2. (c) Model domain and horizontal grid structure of the high-resolution GoM-FVCOM model. The five subregions defined for the regional analysis are also shown. (For interpretation of the references to color in this figure legend, the reader is referred to the web version of this article.)

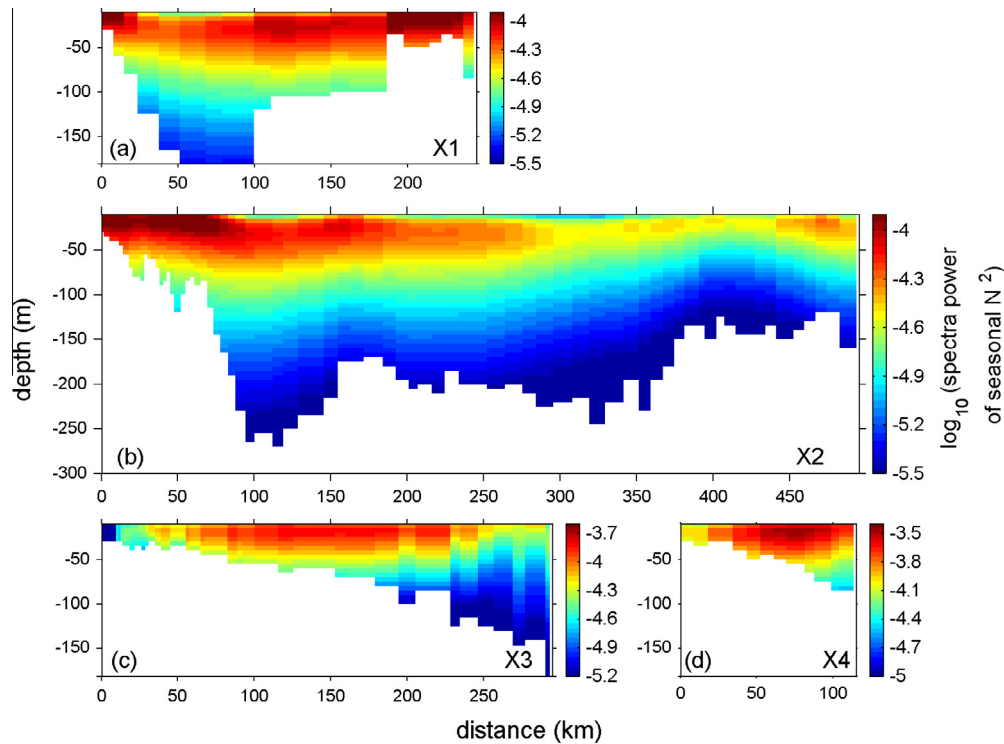


**Fig. A2.** Spectra power of stratification within seasonal band. Locations of 4 cross-shelf sections are shown in Fig. A1b. X-axis is positive eastward across the GoM and southward across the MAB and NSS. To estimate the stratification, Brunt–Väisälä frequency squared [Eq. (1)] is calculated between sea surface and sequential depths toward 500 m with 5 m increment (unit:  $s^{-2}$ ). Color is shown in logarithmic scale. Despite different limits, the range is set same for all colorbars. (For interpretation of the references to color in this figure legend, the reader is referred to the web version of this article.)

within the euphotic zone. Our choice of 0–50 m is consistent with the layer used by Mountain and Manning (1994) in the GoM.

In order to assess whether a reasonable estimation of the ocean state is provided, we compared the reanalysis product with the MARMAP/EcoMon dataset (maintained by the Northeast Fisheries Science Center (NEFSC)) and the Hydrographic Climate Database (maintained by the Bedford Institute of Oceanography (BIO)). These datasets represent the most comprehensive collection of long-term hydrographic measurements on the Northeast U.S. and Nova Scotian shelves. While these data were assimilated by the model, it is important to note that the assimilation does not involve the replacement of model values with observations. Instead, an optimal interpolation is performed aimed at improving model uncertainties that exceed the model's native resolution and within objectively determined spatial (20 km) and temporal windows (3-days). The dataset consists of approximately 48,243 temperature and salinity profiles for the period 1978–2010 ([ftp://ftp.nefsc.noaa.gov/pub/hydro/spool\\_hydro/yearly/](ftp://ftp.nefsc.noaa.gov/pub/hydro/spool_hydro/yearly/) and <http://www.bio.gc.ca/science/data-donnees/base/data-donnees/climate-climate-eng.php>). The overall data coverage is shown as a function of time and location in Fig. A1. Sampling protocols shifted from repeated standard stations to random sampling in the late 1980s, when CTDs replaced water samples and reversing thermometers on NEFSC surveys, and the number of profiles as well as their vertical resolution increased dramatically (Fig. A1a). For the spatial coverage, a majority of profiles were sampled within the 500-m isobath, with some regions receiving much less frequent/dense coverage compared with others (Fig. A1b). Location and resolution checks have been applied prior to the analysis, and profiles must meet the following requirements to be selected: (1) local bathymetry is within the 25–500 m isobaths and (2) vertical measurements are no less than 10 samples. For this, 16.7% of the profiles were

eliminated (a failure of either test causes the whole profile to be rejected).

A point-by-point comparison was conducted whereby the observations were matched with model hindcast estimates at the same time and location (bilinear interpolation was used to map model values from neighboring nodes to the observation site). The metrics for comparison include the stratification defined by three different criteria (Section 'Stratification criteria') and their corresponding temperature and salinity at the sea surface, 50 m depth and sea bottom. The comparison uses multiple quantitative metrics, including the correlation coefficient ( $r$ ), normalized standard deviation ( $NSTD$ ) and normalized root-mean-square difference ( $RMSD$ ), which compare the linear pattern, variation and error of the reanalysis dataset to the in-situ observations, respectively. So a perfect match is reached when the reanalysis data display the same pattern and variation but without any error ( $r = 1$ ,  $NSTD = 1$  and  $RMSD = 0$ ). The comparison of stratification for the period 1978–2010 is summarized in a Taylor Diagram (Taylor, 2001) (Fig. A3, temperature and salinity having similar skill is not shown). The reanalysis product is consistently reliable across all stratification criteria, with  $r = 0.71$ – $0.95$ ,  $NSTD = 0.60$ – $0.93$ , and  $RMSD < 0.71$ , except for moderate underestimation of the variability ( $NSTD < 1$ ) in four subregions. It is expected that the underestimation results from either the model vertical resolution, which is lower than the observations, or the embedded scheme, which tends to smooth the model density profiles. Spatially, the  $NSTD$  is closer to 1 for the three northern subregions than for the SMAB. Relatively higher  $r$  and lower  $RMSD$  are achieved in the three southern subregions compared with the EGoM and NSS regions. The reanalysis product shows similar skill in capturing the stratification regardless of the criteria used for the skill assessment.

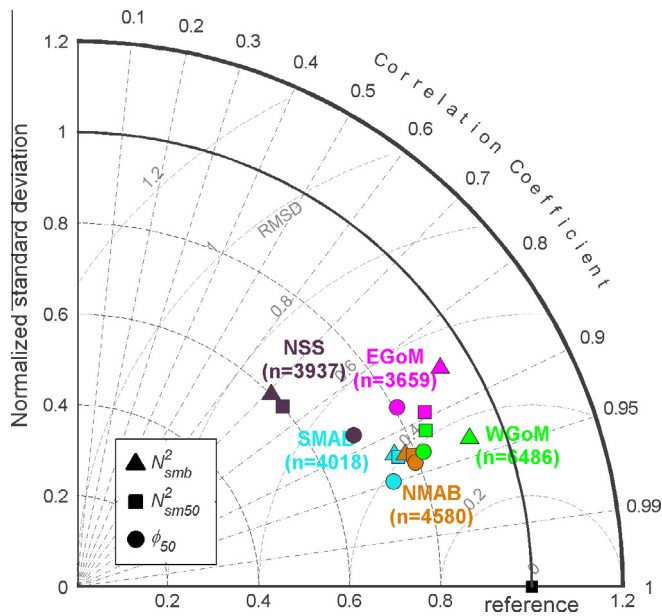


**Fig. A3.** The comparison between stratification calculated from reanalysis dataset and in situ observations. Three statistical quantities are summarized in the Taylor diagram: (1) the correlation coefficient between reanalysis dataset and in-situ observations is indicated on the azimuthal axis; (2) the normalized standard deviation (normalized to the standard deviation of observations) is shown as the distance from the origin of the plot; and (3) the normalized, centered root-mean-square difference (*RMSD*) (normalized to the standard deviation of observations) is shown as the distance from the “reference” point. The colors represent five subregions, while the symbols represent three different stratification criteria, including surface-to-bottom  $N^2_{smb}$ , surface-to-50 m  $N^2_{sm50}$  and surface-to-50 m Simpson Energy  $\phi_{50}$ . A total of 22,680 data points were compared and the number of points (*n*) in each subregion is given. (For interpretation of the references to color in this figure legend, the reader is referred to the web version of this article.)

## References

- Beardsley, R.C., Chapman, D.C., Brink, K.H., Ramp, S.R., Schlitz, R., 1985. The Nantucket Shoals Flux Experiment (NSFE79). Part I: A basic description of the current and temperature variability. *Journal of Physical Oceanography* 15, 713–748.
- Behrenfeld, M.J., 2010. Abandoning Sverdrup's critical depth hypothesis on phytoplankton blooms. *Ecology* 91, 977–989.
- Belkin, I.M., Levitus, S., Antonov, J., Malinberg, S.-A., 1998. “Great salinity anomalies” in the North Atlantic. *Progress in Oceanography* 41, 1–68.
- Boss, E., Behrenfeld, M., 2010. In situ evaluation of the initiation of the North Atlantic phytoplankton bloom. *Geophysical Research Letters*, 37.
- Brody, S.R., Lozier, M.S., Dunne, J.P., 2013. A comparison of methods to determine phytoplankton bloom initiation. *Journal of Geophysical Research: Oceans* 118, 2345–2357.
- Brooks, D.A., Townsend, D.W., 1989. Variability of the coastal current and nutrient pathways in the eastern Gulf of Maine. *Journal of Marine Research* 47, 303–321.
- Bunker, A.F., 1976. Computations of surface energy flux and annual air–sea interaction cycles of the North Atlantic Ocean. *Monthly Weather Review* 104, 1122–1140.
- Burchard, H., 2002. *Applied Turbulence Modelling in Marine Waters*. Springer.
- Butman, B., Beardsley, R.C., 1992. Science in the Gulf of Maine: directions for the 1990s. In: Wiggan, J., Mooers, C.N.K. (Eds.), *Proceedings of the Gulf of Maine Scientific Workshop*, Woods Hole, Massachusetts, 8–10 January 1991. Urban Harbors Institute, University of Massachusetts, Boston, pp. 23–38.
- Carton, J.A., Giese, B.S., 2008. A reanalysis of ocean climate using Simple Ocean Data Assimilation (SODA). *Monthly Weather Review*, 136.
- Castelao, R., Glenn, S., Schofield, O., Chant, R., Wilkin, J., Kohut, J., 2008. Seasonal evolution of hydrographic fields in the central Middle Atlantic Bight from glider observations. *Geophysical Research Letters*, 35.
- Castelao, R., Glenn, S., Schofield, O., 2010. Temperature, salinity, and density variability in the central Middle Atlantic Bight. *Journal of Geophysical Research: Oceans*, 115.
- Chen, C., Liu, H., Beardsley, R.C., 2003. An unstructured grid, finite-volume, three-dimensional, primitive equations ocean model: application to coastal ocean and estuaries. *Journal of Atmospheric and Oceanic Technology* 20, 159–186.
- Chen, C., Beardsley, R.C., Hu, S., Xu, Q., 2005. Using MM5 to hindcast the ocean surface forcing fields over the Gulf of Maine and Georges Bank region. *Journal of Atmospheric & Oceanic Technology*, 22.
- Chen, C., Beardsley, R.C., Luettich, R.A., Westerink, J.J., Wang, H., Perrie, W., Xu, Q., Donahue, A.S., Qi, J., Lin, H., 2013. Extratropical storm inundation testbed: intermodel comparisons in Scituate, Massachusetts. *Journal of Geophysical Research: Oceans* 118, 5054–5073.
- Csanady, G., Hamilton, P., 1988. Circulation of slopewater. *Continental Shelf Research* 8, 565–624.
- Cury, P., Roy, C., 1989. Optimal environmental window and pelagic fish recruitment success in upwelling areas. *Canadian Journal of Fisheries and Aquatic Sciences* 46, 670–680.
- Cushing, D., 1990. Plankton production and year-class strength in fish populations: an update of the match/mismatch hypothesis. *Advances in Marine Biology* 26, 249–293.
- Deese-Riordan, H.E., 2009. *Salinity and Stratification in the Gulf of Maine: 2001–2008*. Vol. Doctor of Philosophy (PhD). The University of Maine, p. 194.
- Drinkwater, K., Gilbert, D., 2004. Hydrographic variability in the waters of the Gulf of St. Lawrence, the Scotian Shelf and the eastern Gulf of Maine (NAFO Subarea 4) during 1991–2000. *Journal of Northwest Atlantic Fishery Science* 34, 85.
- Durbin, E.G., Campbell, R.G., Casas, M.C., Ohman, M.D., Niehoff, B., Runge, J., Wagner, M., 2003. Interannual variation in phytoplankton blooms and zooplankton productivity and abundance in the Gulf of Maine during winter. *Marine Ecology Progress Series* 254, 81–100.
- Ferrari, R., Merrifield, S.T., Taylor, J.R., 2014. Shutdown of convection triggers increase of surface chlorophyll. *Journal of Marine Systems* (in press). <http://dx.doi.org/10.1016/j.jmarsys.2014.02.009>.
- Findlay, H.S., Yool, A., Nodale, M., Pitchford, J.W., 2006. Modelling of autumn plankton bloom dynamics. *Journal of Plankton Research* 28, 209–220.
- Fratantoni, P., Pickart, R., 2003. Variability of the shelf break jet in the Middle Atlantic Bight: internally or externally forced? *Journal of Geophysical Research: Oceans*, 108.
- Fratantoni, P.S., Holzwarth-Davis, T., Bascuñán, C., Taylor, M.H., 2013. Description of the 2012 Oceanographic Conditions on the Northeast U.S. Continental Shelf. NEFSC Reference Document, pp. 13–26.
- Friedland, K.D., Hare, J.A., Wood, G.B., Col, L.A., Buckley, L.J., Mountain, D.G., Kane, J., Brodziak, J., Lough, R.G., Pilskaln, C.H., 2008. Does the fall phytoplankton bloom control recruitment of Georges Bank haddock, *Melanogrammus aeglefinus*, through parental condition? *Canadian Journal of Fisheries and Aquatic Sciences* 65, 1076–1086.
- Gill, A.E., 1982. *Atmosphere-ocean Dynamics*. Academic Press.
- Han, G., Loder, J.W., 2003. Three-dimensional seasonal-mean circulation and hydrography on the eastern Scotian Shelf. *Journal of Geophysical Research: Oceans* 108, 3136.
- Houghton, R., Fairbanks, R., 2001. Water sources for Georges Bank. *Deep Sea Research Part II: Topical Studies in Oceanography* 48, 95–114.
- Hu, S., Chen, C., Ji, R., Townsend, D.W., Tian, R., Beardsley, R.C., Davis, C., 2011. Effects of surface forcing on interannual variability of the fall phytoplankton bloom in the Gulf of Maine revealed using a process-oriented model. *Marine Ecology Progress Series* 427, 29–49.
- Ji, R., Davis, C.S., Chen, C., Townsend, D.W., Mountain, D.G., Beardsley, R.C., 2007. Influence of ocean freshening on shelf phytoplankton dynamics. *Geophysical Research Letters* 34, L24607.
- Ji, R., Davis, C.S., Chen, C., Townsend, D.W., Mountain, D.G., Beardsley, R.C., 2008. Modeling the influence of low-salinity water inflow on winter–spring phytoplankton dynamics in the Nova Scotian Shelf-Gulf of Maine region. *Journal of Plankton Research* 30, 1399–1416.
- Kane, J., 2005. The demography of *Calanus finmarchicus* (Copepoda: Calanoida) in the middle Atlantic bight, USA, 1977–2001. *Journal of Plankton Research* 27, 401–414.
- Kane, J., 2007. Zooplankton abundance trends on Georges Bank, 1977–2004. *ICES Journal of Marine Science* 64, 909–919.
- Kane, J., 2011. Inter-decadal variability of zooplankton abundance in the Middle Atlantic Bight. *Journal of Northwest Atlantic Fishery Science* 43, 81–92.
- Lasker, R., Zweifel, J.R., 1978. Growth and survival of first-feeding northern anchovy larvae (*Engraulis mordax*) in patches containing different proportions of large and small prey. *Spatial Pattern in Plankton Communities*. Springer, pp. 329–354.
- Lentz, S., 2003. A climatology of salty intrusions over the continental shelf from Georges Bank to Cape Hatteras. *Journal of Geophysical Research: Oceans* 108, 3326.
- Lentz, S.J., 2008. Observations and a model of the mean circulation over the Middle Atlantic Bight continental shelf. *Journal of Physical Oceanography* 38, 1203–1221.
- Lentz, S., Shearman, K., Anderson, S., Plueddemann, A., Edson, J., 2003. Evolution of stratification over the New England shelf during the Coastal Mixing and Optics study, August 1996–June 1997. *Journal of Geophysical Research: Oceans* 108, 8–18-14.
- Linder, C.A., Gawarkiewicz, G., 1998. A climatology of the shelfbreak front in the Middle Atlantic Bight. *Journal of Geophysical Research: Oceans* 103, 18405–18423.
- Link, J.S., Brodziak, J.K., Edwards, S.F., Overholtz, W.J., Mountain, D., Jossi, J.W., Smith, T.D., Fogarty, M.J., 2002. Marine ecosystem assessment in a fisheries management context. *Canadian Journal of Fisheries and Aquatic Sciences* 59, 1429–1440.
- Loder, J.W., Petrie, B., Gawarkiewicz, G., 1998. The coastal ocean off northeastern North America: a large-scale view. *The Global Coastal Ocean: Regional Studies and Synthesis*. The Sea 11, 105–133.

- Loder, J.W., Hannah, C.G., Petrie, B.D., Gonzalez, E.A., 2003. Hydrographic and transport variability on the Halifax section. *Journal of Geophysical Research: Oceans* 108, 8003.
- Lozier, M.S., Gawarkiewicz, G., 2001. Cross-frontal exchange in the Middle Atlantic Bight as evidenced by surface drifters. *Journal of Physical Oceanography* 31, 2498–2510.
- Mayer, D.A., Hansen, D.V., Ortman, D.A., 1979. Long-term current and temperature observations on the Middle Atlantic Shelf. *Journal of Geophysical Research: Oceans* 84, 1776–1792.
- Mellor, G.L., Yamada, T., 1982. Development of a turbulence closure model for geophysical fluid problems. *Reviews of Geophysics* 20, 851–875.
- MERCINA Working Group, Greene, C.H., Monger, B.C., McGarry, L.P., Connelly, M.D., Schnepf, N.R., Pershing, A.J., Belkin, I.M., Fratantoni, P.S., Mountain, D.G., Pickart, R.S., 2012. Recent Arctic climate change and its remote forcing of Northwest Atlantic shelf ecosystems. *Oceanography* 25, 208–213.
- Mountain, D.G., 2003. Variability in the properties of Shelf Water in the Middle Atlantic Bight, 1977–1999. *Journal of Geophysical Research: Oceans* 108, 3014.
- Mountain, D.G., Holzwarth, T.J., 1989. Surface and Bottom Temperature Distribution for the Northeast Continental Shelf: US Department of Commerce, National Oceanic and Atmospheric Administration, National Marine Fisheries Service, Northeast Fisheries Center.
- Mountain, D.G., Kane, J., 2010. Major changes in the Georges Bank ecosystem, 1980s to the 1990s. *Marine Ecology Progress Series* 398, 81.
- Mountain, D.G., Manning, J.P., 1994. Seasonal and interannual variability in the properties of the surface waters of the Gulf of Maine. *Continental Shelf Research* 14, 1555–1581.
- Mountain, D.G., Taylor, M.H., Bascuñán, C., 2004. Revised Procedures for Calculating Regional Average Water Properties for Northeast Fisheries Science Center Cruises. NEFSC Reference Document, pp. 04–08.
- Pershing, A.J., Greene, C.H., Jossi, J.W., O'Brien, L., Brodziak, J.K., Bailey, B.A., 2005. Interdecadal variability in the Gulf of Maine zooplankton community, with potential impacts on fish recruitment. *ICES Journal of Marine Science* 62, 1511–1523.
- Petrie, B., Topliss, B.J., Wright, D.G., 1987. Coastal upwelling and eddy development off Nova Scotia. *Journal of Geophysical Research: Oceans* 92, 12979–12991.
- Ramp, S.R., Schlitz, R.J., Wright, W.R., 1985. The deep flow through the Northeast Channel, Gulf of Maine. *Journal of Physical Oceanography* 15, 1790–1808.
- Sharples, J., Ross, O.N., Scott, B.E., Greenstreet, S.P., Fraser, H., 2006. Inter-annual variability in the timing of stratification and the spring bloom in the North-western North Sea. *Continental Shelf Research* 26, 733–751.
- Siegel, D., Doney, S., Yoder, J., 2002. The North Atlantic spring phytoplankton bloom and Sverdrup's critical depth hypothesis. *Science* 296, 730–733.
- Simpson, J.H., Brown, J., Matthews, J., Allen, G., 1990. Tidal straining, density currents, and stirring in the control of estuarine stratification. *Estuaries* 13, 125–132.
- Smagorinsky, J., 1963. General circulation experiments with the primitive equations: I. The basic experiment\*. *Monthly Weather Review* 91, 99–164.
- Smith, P.C., 1983. The mean and seasonal circulation off southwest Nova Scotia. *Journal of Physical Oceanography* 13, 1034–1054.
- Smith, P.C., 1989. Seasonal and interannual variability of current, temperature and salinity off southwest Nova Scotia. *Canadian Journal of Fisheries and Aquatic Sciences* 46, s4–s20.
- Smith, P.C., Houghton, R.W., Fairbanks, R.G., Mountain, D.G., 2001. Interannual variability of boundary fluxes and water mass properties in the Gulf of Maine and on Georges Bank: 1993–1997. *Deep Sea Research Part II: Topical Studies in Oceanography* 48, 37–70.
- Song, H., Ji, R., Stock, C., Wang, Z., 2010. Phenology of phytoplankton blooms in the Nova Scotian Shelf-Gulf of Maine region: remote sensing and modeling analysis. *Journal of Plankton Research* 32, 1485–1499.
- Song, H., Ji, R., Stock, C., Kearney, K., Wang, Z., 2011. Interannual variability in phytoplankton blooms and plankton productivity over the Nova Scotian Shelf and in the Gulf of Maine. *Marine Ecology Progress Series* 426, 105–133.
- Sullivan, M.C., Cowen, R.K., Steves, B.P., 2005. Evidence for atmosphere–ocean forcing of yellowtail flounder (*Limanda ferruginea*) recruitment in the Middle Atlantic Bight. *Fisheries Oceanography* 14, 386–399.
- Sverdrup, H., 1953. On conditions for the vernal blooming of phytoplankton. *ICES Journal of Marine Science* 18, 287–295.
- Taylor, K.E., 2001. Summarizing multiple aspects of model performance in a single diagram. *Journal of Geophysical Research: Atmospheres* 106, 7183–7192.
- Taylor, M.H., Mountain, D.G., 2009. The influence of surface layer salinity on wintertime convection in Wilkinson Basin, Gulf of Maine. *Continental Shelf Research* 29, 433–444.
- Townsend, D.W., 1998. Sources and cycling of nitrogen in the Gulf of Maine. *Journal of Marine Systems* 16, 283–295.
- Umoh, J.U., Loder, J.W., Petrie, B., 1995. The role of air–sea heat fluxes in annual and interannual ocean temperature variability on the eastern Newfoundland shelf. *Atmosphere-Ocean* 33, 531–568.
- Weinberg, J.R., 2005. Bathymetric shift in the distribution of Atlantic surfclams: response to warmer ocean temperature. *ICES Journal of Marine Science* 62, 1444–1453.
- Xu, Y., Chant, R., Gong, D., Castelao, R., Glenn, S., Schofield, O., 2011. Seasonal variability of chlorophyll a in the Mid-Atlantic Bight. *Continental Shelf Research* 31, 1640–1650.
- Yamada, K., Ishizaka, J., 2006. Estimation of interdecadal change of spring bloom timing, in the case of the Japan Sea. *Geophysical Research Letters*, 33.
- Zhang, W.G., Wilkin, J.L., Chant, R.J., 2009. Modeling the pathways and mean dynamics of river plume dispersal in the New York Bight. *Journal of Physical Oceanography*, 39.